IOWA STATE UNIVERSITY
Digital Repository

2-21-2017

Impact of phase transition sequence on the electrocaloric effect in Pb(Nb,Zr,Sn,Ti)O-3 ceramics

Zunping Xu
Iowa State University

Zhongming Fan
Iowa State University, zfanad@iastate.edu

Xiaoming Liu
Iowa State University

Xiaoli Tan
Iowa State University, xtan@iastate.edu

Impact of phase transition sequence on the electrocaloric effect in Pb(Nb,Zr,Sn,Ti)O-3 ceramics

Abstract

The phase transition sequence in PbZrO3-based ceramics can be readily altered by chemical modification. In Pb0.99Nb0.02[(Zr0.57Sn0.43)(0.92)Ti-0.08](0.98)O-3 (PNZST 43/8/2), the sequence is ferroelectric-antiferroelectric-paraelectric during heating, while in Pb0.99Nb0.02 (Zr0.85Sn0.13Ti0.02)(0.98)O-3 (PNZST 13/2/2), it is antiferroelectric-ferroelectric-paraelectric during heating. The electrocaloric effect associated with the antiferroelectricferroelectric phase transition is studied in both ceramics via indirect measurement. PNZST 43/8/2 is observed to display a positive electrocaloric effect; in contrast, PNZST 13/2/2 exhibits a negative effect.

Keywords

Ceramics, Ferroelectric phase transitions, Dielectric properties, Polarization, Antiferroelectric phase transitions

Disciplines

Ceramic Materials | Materials Science and Engineering

Comments

Impact of phase transition sequence on the electrocaloric effect in Pb(Nb,Zr,Sn,Ti)O$_3$ ceramics

Zunping Xu,[1,2] Zhongming Fan,[1] Xiaoming Liu,[1] and Xiaoli Tan[1,a]

[1]Department of Materials Science and Engineering, Iowa State University, Ames, Iowa 50011, USA
[2]Faculty of Materials and Energy, Southwest University, Chongqing 400715, China

The phase transition sequence in PbZrO$_3$-based ceramics can be readily altered by chemical modification. In Pb$_{0.99}$Nb$_{0.02}$[(Zr$_{0.57}$Sn$_{0.43}$)$_{0.92}$Ti$_{0.08}$]$_{0.98}$O$_3$ (PNZST 43/8/2), the sequence is ferroelectric–antiferroelectric–paraelectric during heating, while in Pb$_{0.99}$Nb$_{0.02}$(Zr$_{0.85}$Sn$_{0.13}$Ti$_{0.02}$)$_{0.98}$O$_3$ (PNZST 13/2/2), it is antiferroelectric–ferroelectric–paraelectric during heating. The electrocaloric effect associated with the antiferroelectric $\leftrightarrow$ ferroelectric phase transition is studied in both ceramics via indirect measurement. PNZST 43/8/2 is observed to display a positive electrocaloric effect; in contrast, PNZST 13/2/2 exhibits a negative effect. *Published by AIP Publishing.* [http://dx.doi.org/10.1063/1.4976827]

The electrocaloric effect, thermodynamically equivalent to the pyroelectric effect, describes the coupling between electrical and thermal properties in polar crystals.[1] Strong couplings, manifesting in large temperature changes upon application of electric fields under adiabatic conditions, have been reported in a variety of ceramics[2–7] and some polymers.[4,8] A large electrocaloric effect is always associated with phase transitions.[9–11]

Antiferroelectric ceramics are known to be rich in phase transitions.[12–16] Indeed, they are unrivaled among all reported materials in terms of their ultrahigh temperature changes.[3,17] In particular, a record value of 45.3 °C under ~600 kV/cm was reported in an antiferroelectric Pb$_{0.8}$Zr$_{0.2}$O$_3$ thin film.[18] It is interesting to note that antiferroelectrics can also exhibit a negative electrocaloric effect.[19,20] This was hypothesized to be caused by the entropy increase resulting from the distinct responses of the two antiferroelectric sublattices to an applied electric field.[20]

Based only on the Maxwell relationship, without consideration of any microscopic mechanisms, a negative electrocaloric effect should be expected in any materials with positive temperature coefficients of their polarizations. Most PbZrO$_3$-based compositions display a sequence of ferroelectric–antiferroelectric–paraelectric phase transitions during heating.[12–16] Since the antiferroelectric phase is non-polar, the polarization, either spontaneous or induced, decreases with temperature in the vicinity of the ferroelectric–antiferroelectric phase transition. In consequence, a conventional (positive) electrocaloric effect is anticipated in these compounds. In certain chemically modified PbZrO$_3$ compositions,[12,17,21] the phase transition sequence during heating becomes antiferroelectric–ferroelectric–paraelectric. These compositions are expected to display a positive temperature coefficient of polarization and, hence, a negative electrocaloric effect. To corroborate this speculation, the electrocaloric effect in two antiferroelectric ceramics with opposite phase transition sequences is evaluated via indirect measurements in the present work.

Based on previous studies,[12,22–24] two compositions, Pb$_{0.99}$Nb$_{0.02}$(Zr$_{0.85}$Sn$_{0.13}$Ti$_{0.02}$)$_{0.98}$O$_3$, abbreviated as PNZST 13/2/2, and Pb$_{0.99}$Nb$_{0.02}$[(Zr$_{0.57}$Sn$_{0.43}$)$_{0.92}$Ti$_{0.08}$]$_{0.98}$O$_3$, abbreviated as PNZST 43/8/2, are selected for investigation. The PNZST 13/2/2 ceramic was fabricated using the solid state reaction method. Powders of PbO, ZrO$_2$, SnO$_2$, TiO$_2$, and Nb$_2$O$_5$ with purity levels >99.9% were batched with an additional 5 wt. % PbO to compensate for PbO evaporation during calcination and sintering. Calcination was repeated twice at 935 °C for 2 h for compositional homogeneity. Calcined powders with an acrylic binder were uniaxially pressed into disks and sintered at 1350 °C for 3 h in air using a double crucible configuration with protective powder. The PNZST 43/8/2 ceramic was fabricated in a similar manner but with a post sintering hot isostatic pressing at 1150 °C and ~200 MPa for 2 h in a 20% O$_2$ and 80% Ar atmosphere.[24] The crystal structures of the ceramics were analyzed with an X-ray diffractometer (Model D500, Siemens, Germany). A scanning electron microscope (SEM, FEI Quanta 250) was used to examine the grain size and morphology of the ceramics. The ceramic density was measured by the Archimedes method. The heat capacity of the ceramic was measured using a differential scanning calorimeter (DSC, Q2000, TA Instruments). For electrical measurements, silver electrodes were sputtered on the specimen surface. The dielectric properties as a function of temperature were measured during heating and cooling at a rate of 3 °C/min using an LCZ meter (Keithley 3330). The polarization vs. electric field hysteresis loops at different temperatures were measured by using a standardized ferroelectric test system (RT-66 A, Radiant Technologies). Prior to recording the data at each temperature, the specimen was held for at least five minutes to ensure a uniform temperature.

X-ray diffraction indicates that both ceramics are phase pure with distorted perovskite structures (Fig. 1). The PNZST 43/8/2 ceramic exhibits a tetragonal distortion at room temperature, while the PNZST 13/2/2 ceramic is in an orthorhombic phase. This result is consistent with previous studies.[12,17] For simplicity, the diffraction peaks are indexed according to a pseudo-cubic perovskite structure.

Figure 2 shows the SEM micrographs of the fracture surface of both ceramics. Some pores are visible in the

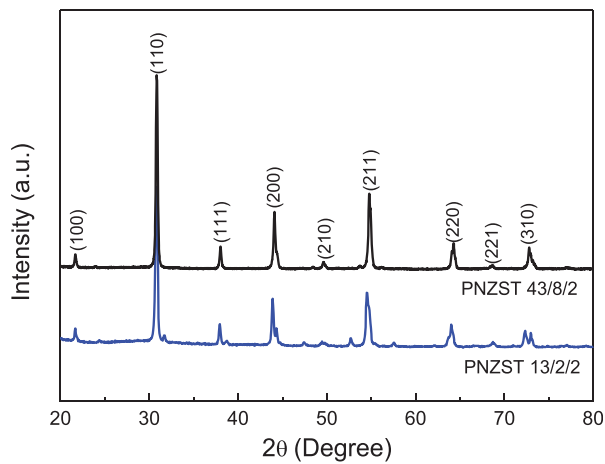a)Author to whom correspondence should be addressed. Electronic mail: xtan@iastate.edu

FIG. 1. X-ray diffraction patterns of the PNZST 13/2/2 and PNZST 43/8/2 ceramics.

PNZST 13/2/2 ceramic. The average grain size is determined to be 2.48 μm using the linear intercept method. The PNZST 43/8/2 ceramic is almost free of pores because of the additional step of hot isostatic pressing. The average grain size is 2.60 μm. The density measurement results, showing a 94% relative density for PNZST 13/2/2 and 99% for PNZST 43/8/2, support the SEM observation.

The temperature dependence of the dielectric constant, ε_r, at 1 kHz for both ceramics during heating and cooling, is shown in Fig. 3. The anomalies on the ε_r vs. T curves indicate phase transition temperatures. PNZST 13/2/2 is antiferroelectric at room temperature, which transforms to ferroelectric at $\sim$110 °C and then to paraelectric at $\sim$172 °C during heating. Upon cooling, the paraelectric to ferroelectric transition occurs at $\sim$171 °C, while the ferroelectric to antiferroelectric transition takes place around 88 °C. In contrast, the ferroelectric phase in PNZST 43/8/2 is the low temperature phase. The ceramic transforms into the antiferroelectric phase at about 43 °C during heating and then to the paraelectric phase at $\sim$135 °C. On cooling, the reverse phase transitions take place at $\sim$134 °C and -8 °C, respectively. As anticipated, the two compositions display opposite antiferroelectric $\leftrightarrow$ ferroelectric phase transition sequences during temperature change. It is also interesting to note that this phase transition displays quite a large thermal hysteresis, 22 °C for PNZST 13/2/2 and 51 °C for PNZST 43/8/2.

In order to evaluate the electrocaloric effect, the electric field-induced polarization, $P(E)$, was measured at a series of temperatures with a 10 °C interval. For PNZST 13/2/2, the P-
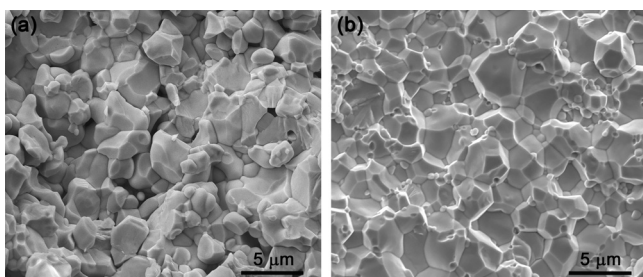

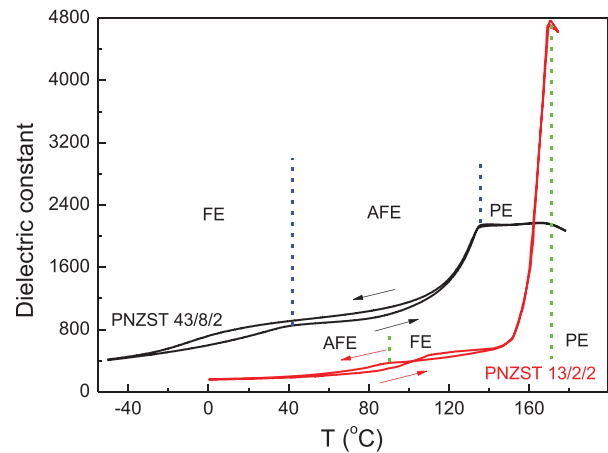FIG. 2. SEM micrographs of fractured surfaces of the (a) PNZST 13/2/2 and (b) PNZST 43/8/2 ceramics.

FIG. 3. Temperature dependence of the dielectric constant at 1 kHz for the PNZST 13/2/2 and PNZST 43/8/2 ceramics upon heating and cooling. The green dashed lines delineate the different phases during cooling of PNZST 13/2/2 and the blue dashed lines delineate those during heating of PNZST 43/8/2. AFE: antiferroelectric; FE: ferroelectric; and PE: paraelectric.

E loops were recorded under applied electric fields of the peak value of 130 kV/cm from 0 to 160 °C during the heating sequence. Meanwhile, for PNZST 43/8/2, the measurement was conducted under the peak field of 90 kV/cm between -30 and 130 °C during the cooling sequence. Different sequences were used for the two ceramics in order to minimize any possible history effect.[3] Representative P-E hysteresis loops for both ceramics are displayed in Fig. 4. It is evident that a single hysteresis loop, indicating the ferroelectric state, is seen at higher temperatures in PNZST 13/2/2 but at lower
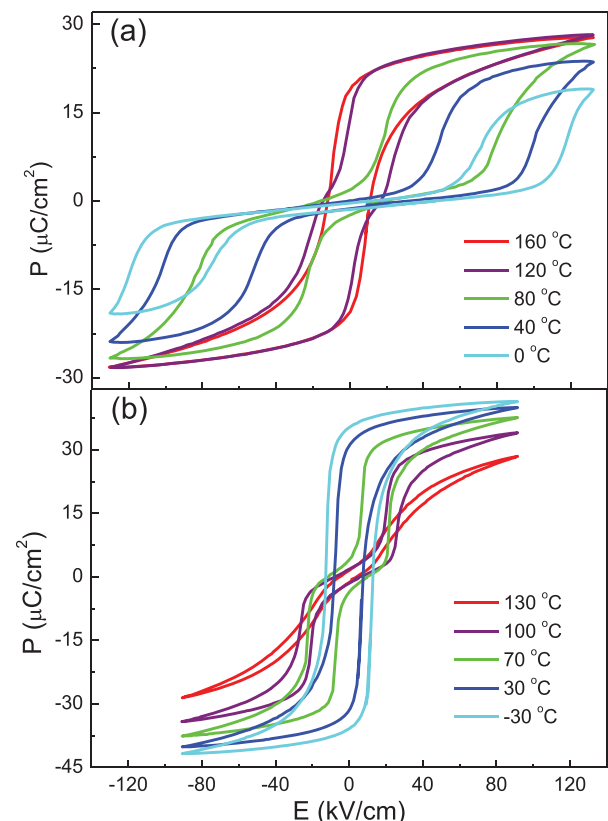

FIG. 4. Polarization, P, vs. electric field, E, hysteresis loops at selected temperatures for the (a) PNZST 13/2/2 and (b) PNZST 43/8/2 ceramics.
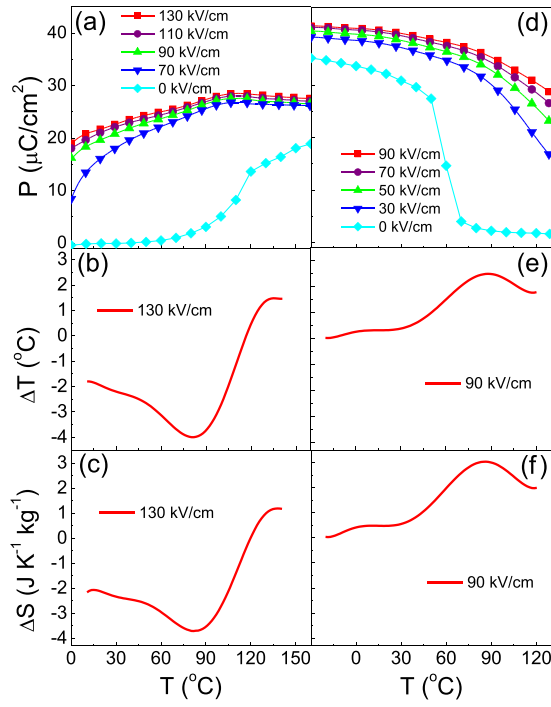
FIG. 5. Polarization at selected fields from measured *P-E* hysteresis loops for (a) PNZST 13/2/2 and (d) PNZST 43/8/2. Calculated temperature change ΔT and entropy change ΔS for (b) and (c) PNZST 13/2/2 and (e) and (f) PNZST 43/8/2, respectively.

temperatures in PNZST 43/8/2. Double hysteresis loops, signifying an antiferroelectric state, are observed at lower temperatures in PNZST 13/2/2 but at higher temperatures in PNZST 43/8/2. The polarization measurement, therefore, confirms the opposite phase transition sequences in these two ceramics.

The polarization data (*P*), extracted from the upper branches of the *P-E* hysteresis loops in the range of $E \geq 0$, as a function of temperature are shown in Figs. 5(a) and 5(d). The data at 0 kV/cm represent the temperature evolution of the remanent polarization. It can be observed that the remanent polarization starts quickly increasing at 90 °C in PNZST 13/2/2 and precipitously dropping at 50 °C in PNZST 43/8/2. This agrees well with the phase transition temperatures revealed by the dielectric constant measurement (Fig. 3). Furthermore, the *P* vs. *T* curves display a positive slope for PNZST 13/2/2 throughout the majority of the measurement temperature range and a negative slope for PNZST 43/8/2 for the entire temperature range. Even though the polarization at high fields is a result of the electric field-induced ferroelectric phase, the opposite slopes are apparently rooted in the antiferroelectric phase, being stable at lower temperatures in PNZST 13/2/2 and at higher temperatures in PNZST 43/8/2.

Following the procedure described in Ref. 3, the electrocaloric temperature change (ΔT) and entropy change (ΔS) are calculated according to

$$\Delta T = -\frac{1}{C\rho} \int_{E_1}^{E_2} T \left(\frac{\partial P}{\partial T} \right)_E dE, \qquad (1)$$

$$\Delta S = -\frac{1}{\rho} \int_{E_1}^{E_2} \left(\frac{\partial P}{\partial T} \right)_E dE, \qquad (2)$$

where *P* is the polarization, ρ is the mass density, and *C* is the heat capacity. The quantity $\frac{\partial P}{\partial T}$, the temperature coefficient of the polarization, is obtained from the sixth-order polynomial fit to the *P*(*T*) data. In the present work, the mass density is 7.78 g·cm^{-3} for PNZST 13/2/2 and 8.24 g·cm^{-3} for PNZST 43/8/2. The heat capacity is assumed to be a constant within the measurement temperature window and is taken to be 330 J·K^{-1}·kg^{-1} for PNZST 13/2/2 and 440 J·K^{-1}·kg^{-1} for PNZST 43/8/2. The integral is performed between $E_1 = 0$ and E_2, the peak field (130 kV/cm for PNZST 13/2/2 and 90 kV/cm for PNZST 43/8/2). The ΔT and ΔS profiles at lower electric fields are not calculated for PNZST 13/2/2 because the antiferroelectric to ferroelectric phase transition does not occur at lower electric fields in the lower part of the temperature window and the corresponding polarization values cannot be extracted from the loops measured at 130 kV/cm. For the sake of consistent presentation, ΔT and ΔS profiles are also only calculated at the peak field for PNZST 43/8/2. The results for PNZST 13/2/2 are displayed in Figs. 5(b) and 5(c) and those for PNZST 43/8/2 in Figs. 5(e) and 5(f). A negative ΔT peak is observed for PNZST 13/2/2, and, in contrast, a positive ΔT peak is observed for PNZST 43/8/2. Under the applied field of 130 kV/cm, a maximum ΔT value of -4.0 °C is obtained for the PNZST 13/2/2 ceramic at $\sim$82 °C [Fig. 5(b)]. For the PNZST 43/8/2 ceramic, the maximum ΔT of 2.5 °C is observed at 88 °C under a field of 90 kV/cm.

It should be made clear that these values of ΔT, derived from the indirect method, exclude the contribution of the latent heat of the first order antiferroelectric-to-ferroelectric phase transition.[25] Additional DSC tests show that the antiferroelectric-to-ferroelectric transition is endothermic in PNZST 13/2/2 but exothermic in PNZST 43/8/2. This suggests that the electric field induced antiferroelectric-to-ferroelectric transition under adiabatic conditions leads to a temperature decrease in PNZST 13/2/2 but an increase in PNZST 43/8/2. In other words, the latent heat works in synergy with the negative electrocaloric effect in PNZST 13/2/2 and with the positive effect in PNZST 43/8/2 from the induced ferroelectric phase. Therefore, the indirect method faithfully reveals the sign of temperature change but underestimates its values in both ceramics. Direct measurements are expected to show larger temperature changes.[26] It is of interest for potential device applications to verify the temperature change in these two ceramics with the direct method in future studies.

Along with the main peak in ΔT, PNZST 43/8/2 also displays a minor peak at $\sim$5 °C [Fig. 5(e)]. It is plausible to attribute this feature to the existing ferroelectric phase prior to the application of electric field. To support this argument, additional indirect electrocaloric measurements were conducted between -30 and 130 °C during the heating sequence. Compared to the cooling sequence data in Fig. 5(e), the minor peak in ΔT becomes stronger, while the main peak remains unchanged in the heating sequence (data not shown). The ferroelectric and antiferroelectric phases coexist in PNZST 43/8/2 between -8 °C and 43 °C (Fig. 3). Close to the lower end of this temperature window, the fraction of the ferroelectric phase is lower in the cooling sequence than in the heating sequence, leading to a weaker ΔT peak at $\sim$5 °C in the cooling sequence.

Our comparative investigations of the electrocaloric effect in PNZST 13/2/2 and PNZST 43/8/2 using an indirect method demonstrate the impact of the antiferroelectric ↔ ferroelectric phase transition sequence on the sign of electrocaloric temperature change (ΔT). In the vicinity of the transition temperature, materials that transform from an antiferroelectric state to a ferroelectric state upon heating are expected to develop larger field-induced polarization at higher temperatures. A positive temperature coefficient of polarization produces a negative electrocaloric effect. However, for reasons unknown to us, the negative electrocaloric effect was not reported in previous studies in this category of materials.[17,18] In previous reports on negative electrocaloric effects, the ΔT peak was observed deep in the antiferroelectric region at temperatures far from critical temperatures,[19] and the interpretation involves only the antiferroelectric phase with different field responses of the two sublattices.[20] In our present work, not only is the ΔT peak observed at temperatures close to the antiferroelectric ↔ ferroelectric transition temperature but also both ceramics are at the ferroelectric state (poled or field-induced) under high fields within the measurement temperature range. To elucidate the exact reason why the ferroelectric phases exhibit different temperature dependencies of polarization in materials with opposite temperature-induced antiferroelectric ↔ ferroelectric transition sequences, theoretical insights using *ab initio* calculations will be required.

In summary, the electrocaloric effect is investigated via the indirect method on bulk samples of two chemically modified $PbZrO_3$ compositions. The direct impact of the antiferroelectric ↔ ferroelectric phase transition on the electrocaloric temperature change is demonstrated. In PNZST 13/2/2, where the antiferroelectric phase exists at temperatures below the ferroelectric phase, a negative effect is observed. In PNZST 43/8/2, where the antiferroelectric phase exists at temperatures above the ferroelectric phase, a positive effect is seen.

[1] R. E. Newnham, *Properties of Materials*: *Anisotropy*, *Symmetry, Structure* (Oxford Univ. Press, New York, 2005).

[2] B. A. Tuttle and D. A. Payne, Ferroelectrics **37**, 603 (1981).

[3] A. S. Mischenko, Q. Zhang, J. F. Scott, R. W. Whatmore, and N. D. Mathur, Science **311**, 1270 (2006).

[4] S. G. Lu, B. Rozic, Q. M. Zhang, Z. Kutnjak, X. Y. Li, E. Furman, L. J. Gorny, M. R. Lin, B. Malic, M. Kosec, R. Blinc, and R. Pirc, Appl. Phys. Lett. **97**, 162904 (2010).

[5] X. Wang, F. Tian, C. Zhao, J. Wu, Y. Liu, and B. Dkhil, Appl. Phys. Lett. **107**, 252905 (2015).

[6] Y. B. Ma, K. Albe, and B. X. Xu, Phys. Rev. B **91**, 184108 (2015).

[7] X. S. Qian, H. J. Ye, Y. T. Zhang, H. Gu, X. Li, C. A. Randall, and Q. M. Zhang, Adv. Funct. Mater. **24**, 1300 (2014).

[8] B. Neese, B. J. Chu, S. G. Lu, Y. Wang, E. Furman, and Q. M. Zhang, Science **321**, 821 (2008).

[9] X. Moya, S. Kar-Narayan, and N. D. Mathur, Nature Mater. **13**, 439 (2014).

[10] Y. Liu, J. F. Scott, and B. Dkhil, APL Mater. **4**, 064109 (2016).

[11] F. Weyland, M. Acosta, J. Koruza, P. Breckner, J. Rödel, and N. Novak, Adv. Funct. Mater. **26**, 7326 (2016).

[12] D. Berlincourt, IEEE Trans. Sonics Ultrason. **SU13**, 116 (1966).

[13] W. Pan, Q. Zhang, A. Bhalla, and L. E. Cross, J. Am. Ceram. Soc. **72**, 571 (1989).

[14] D. Viehland, D. Forst, Z. Xu, and J. F. Li, J. Am. Ceram. Soc. **78**, 2101 (1995).

[15] H. He and X. Tan, Phys. Rev. B **72**, 024102 (2005).

[16] X. Tan, C. Ma, J. Frederick, S. Beckman, and K. G. Webber, J. Am. Ceram. Soc. **94**, 4091 (2011).

[17] X. Hao and J. Zhai, Appl. Phys. Lett. **104**, 022902 (2014).

[18] B. Peng, H. Fan, and Q. Zhang, Adv. Funct. Mater. **23**, 2987 (2013).

[19] R. Pirc, B. Rozic, J. Koruza, B. Malic, and Z. Kutnjak, Europhys. Lett. **107**, 17002 (2014).

[20] W. Geng, Y. Liu, X. Meng, L. Bellaiche, J. F. Scott, B. Dkhil, and A. Jiang, Adv. Mater. **27**, 3165 (2015).

[21] B. P. Pokharel and D. Pandey, J. Appl. Phys. **88**, 5364 (2000).

[22] Z. Xu, J. Zhai, and W. H. Chan, Appl. Phys. Lett. **88**, 132908 (2006).

[23] X. Tan, J. Frederick, C. Ma, W. Jo, and J. Rödel, Phys. Rev. Lett. **105**, 255702 (2010).

[24] X. Tan, S. E. Young, Y. H. Seo, J. Y. Zhang, W. Hong, and K. G. Webber, Acta Mater. **62**, 114 (2014).

[25] Y. Liu, J. F. Scott, and B. Dkhil, Appl. Phys. Rev. **3**, 031102 (2016).

[26] M. Sanlialp, V. V. Shvartsman, M. Acosta, and D. C. Lupascu, J. Am. Ceram. Soc. **99**, 4022 (2016).